PCCP

Accepted Manuscript

ROYAL SOCIETY OF CHEMISTRY

www.rsc.org/pccp

DOS and electron attachment effects in the electron-induced vibrational excitation of terphenylthiol SAMs

J. Houplin[1,2], L. Amiaud[1,2], C. Dablemont[1,2], A. Lafosse[1,2]

[1] *Univ Paris-Sud, Institut des Sciences Moléculaires d'Orsay (ISMO), UMR 8214, Orsay, F-91405*
[2] *CNRS, Orsay, F-91405*

Abstract

Low energy electron scattering on terphenylthiol (TPT, HS-$(C_6H_4)_2$-C_6H_5) self-assembled monolayers (SAMs) deposited onto gold was investigated using high resolution electron energy loss spectroscopy (HREELS) by recording specular elastic and inelastic excitation functions. The electron elastic reflectivity could be directly compared to the sample density-of-states (DOS) above vacuum level. A high reflectivity region was observed in the range 7.2-8.6 eV. Inelastic excitation functions were studied to get insights into the mechanisms involved in the excitation of a selection of vibrational modes (dipolar and impact scattering). In particular, a resonant mechanism was observed in the excitation of the stretching mode ν(CC) at 196 meV. The purely resonant contribution to the electron-induced excitation of the stretching modes ν(CH) (379 meV) could be extracted from the overtone excitation. It is located at 7.2 eV above the vacuum level and is characterized by a width of 3.4 eV.

Graphical abstract

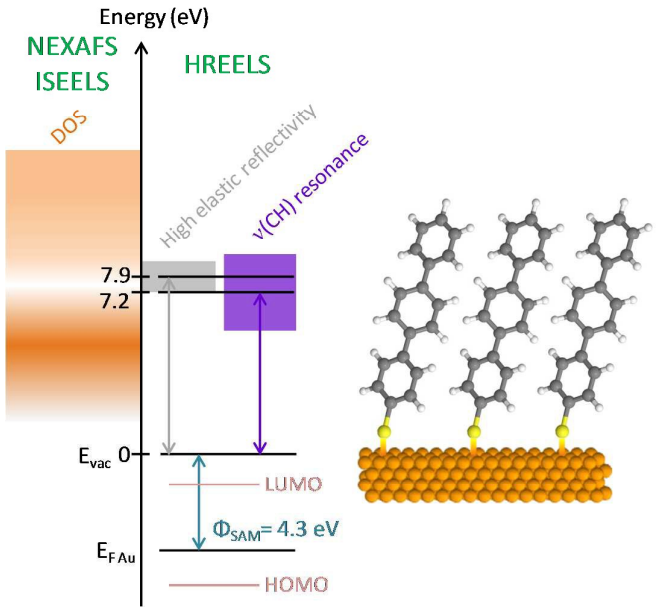

1. Introduction

Self-assembled monolayers (SAMs) are promising molecular systems, often used as resists to develop sensors [1, 2] and functionalized carbon nanomembranes [3, 4]. Many developed irradiation-assisted chemical lithography processes rely on the increase of the aromatic system stability through cross-linking [4-6]. Low-energy electrons, being primary as well as secondary electrons created when working at high incident energies [7, 8], initiate efficient reactive processes and contribute to the overall chemical transformation induced by irradiation of the resist. Interaction mechanisms of the electron-molecular system have relative probabilities which depend strongly on the energy of the electrons [9-11]. In particular, below 15 eV, dissociative electron attachment (DEA) processes take place. They proceed through the formation of transient negative ions (TNI), which decay following two competitive pathways. On the one hand, the molecular systems can dissociate, which leads to the formation of targeted reactive species within the SAM and subsequent chemical processes. On the other hand, TNIs can evolve by electron autodetachment, which leaves the systems into vibrationally excited states. Thus, probing the vibrational excitation mechanisms is a way to look for and identify electron attachment resonances, which might later on be used to induce controlled chemistry.

Self-Assembled Monolayers of *p*-terphenylthiol HS-$(C_6H_4)_2$-C_6H_5 (TPT) deposited onto gold can serve as model systems for aromatic lithography resists. This work belongs to a series of papers dealing with pristine and electron irradiated TPT SAMs, which were mostly probed by high resolution electron energy loss spectroscopy (HREELS). Energy loss spectra were recorded at different incident electron energies. The observed losses were attributed to the excitation of fundamental vibrational modes, based on DFT calculations performed on the isolated molecules [12]. An interesting series of overtones was observed at about 6 eV, which allowed modelling the unresolved stretching mode ν(CH) behaviour by a 1D anharmonic oscillator. This type of overtone series is one of the signature for vibrational excitation through electron attachment. A further proof for this attachment process was the broad bell-shape peak observed in the excitation function recorded for the associated loss feature at 378 meV [13]. One of the aims of that study was to demonstrate the vibrational mode selectivity of the involved resonance. The spectrometer transmission function was optimized at low energy in order to smooth away any possible density-of-states (DOS) induced structures. By contrast, in the present study, the spectrometer is optimized at high energy, so that the instrument function is unstructured within the probed energy region. After a careful

energy calibration (presented in section 2), elastic reflectivity measurements are performed to probe the sample DOS above vacuum level [14, 15]. The agreement between the DOS structures deduced for TPT SAMs by HREELS and near-edge X-ray absorption fine structure (NEXAFS) [16-20] with the ones observed for gaseous benzene using inner-shell electron energy loss (ISEEL) [21] is striking (section 3.1). Vibrational excitation mechanisms (dipolar and impact scattering) are discussed for a selection of 11 energy losses, ascribed to fundamental and multiple losses (section 3.2). Particular attention is paid to the ν(CH) resonance already identified at 6 eV. Thanks to the energy calibration, this resonance can be located at 7.2 eV above the vacuum level (FWHM = 3.4 eV), and its nature is discussed considering the comprehensive set of data available in the literature for gaseous benzene.

2. Experimental part

SAMs preparation. The 1,1,4',1"-terphenyl-4-thiol (TPT, HS-$(C_6H_4)_2$-C_6H_5) SAMs preparation and characterization were described in detail in a previous paper [13]. TPT was purchased from Sigma-Aldrich (97%, Saint-Quentin Fallavier, France). All solvents were reagent grade. Reagents were used without any further purification. Experiments were carried out at room temperature. Glass substrates (11 mm×11 mm) coated successively with a 2.5 nm thick layer of chromium and a 250 nm thick layer of gold were purchased from Arrandee (Werther, Germany) [22]. The gold-coated substrates were annealed by a brief passage in a flame, then cleaned by 30 minutes of UV-Ozone. The substrates were immersed in freshly prepared saturated solutions of thiol in absolute ethanol at a thiol concentration of ~1 mM for 2 hours under stirring. After thorough rinsing in ethanol (15 minutes), the surfaces were rinsed in milliQ water for 15 minutes then dried under a flow of dry nitrogen.

HREELS characterization of SAMs. The HREEL spectrometer, specially designed to measure energy loss spectra as well as excitation functions, is housed in a dedicated UHV experimental setup (base pressure kept below 2 x 10^{-10} mbar). The SAMs are loaded into the system through a load-lock chamber that allows their transfer into UHV at room temperature, without baking the vacuum chambers.

The HREEL spectrometer consists of a double monochromator and a single analyzer (model IB 500 by Omicron). All the presented spectra were measured at room temperature and in the specular geometry ($\theta_i = \theta_f = 55°$ with respect to the surface normal). Electron energy loss spectra $I = I(E_{loss})$ were recorded at fixed incident electron energy E_i, with an overall resolution ΔE_{FWHM} ~ 7-8 meV, measured as the full width at half maximum (FWHM) of the

elastic peak. The number of detected electrons is measured as a function of the energy E_{loss} they have lost upon scattering on the sample. Spectra measured over the extended range $-15 \leq E_{loss} \leq 1200$ meV were discussed in detail in a previous publication [12].

Quasi-elastic (i.e. elastic reflectivity) and inelastic (i.e. vibrational) excitation functions $I = I(E_i)$ are acquired quasi-continuously over the energy range 5–13 eV (typical step of 0.1 eV). The general trends appear much clearly than what would be visible following a step-by-step acquisition procedure. Excitation functions are recorded by following the variation of the number of detected electrons having lost the considered amount of energy E_{loss} upon surface scattering. The peak count rate given in number of counts per second is followed as a function of the incident electron energy E_i. The elastic reflectivity curve corresponds to the particular case $E_{loss} \approx 0$ meV. The recorded excitation functions are modulated by the instrument transmission function, which depends on the electron energy chosen for the initial spectrometer optimization (called optimization energy). The optimization procedure is the following. For a selected initial energy, all the spectrometer potentials are tuned and the sample position in the HREELS collision chamber is adjusted under the criterion of maximizing the intensity of the elastic peak while keeping a good resolution ($\Delta E_{FWHM} \sim$ 7-8 meV). Then, for a set of incident energies E_i, only the potentials applied to the focussing lenses located at the exit of the second monochromator and at the entrance of the analyser are varied in order to maximize the elastic intensity, keeping the resolution constant within ± 1 meV. Linear variation laws are derived from the resulting potential values and are used to extrapolate the optimal lens values over the whole energy range. They are fed into the acquisition software for (in)elastic excitation function recording, while the position of the sample is kept unchanged. The incident electron energy range that can be covered is determined by the limits for elastic intensity extinction, which are most often accompanied by a degradation of the resolution. In order to assess the instrument transmission function effects, the sample position, initial energy and spectrometer potentials are varied. The excitation functions obtained after these distinct optimization procedures have to be confronted each other.

To evaluate a possible charging effect during measurement, excitation functions were recorded either by increasing or decreasing incident electron energies E_i. The representative (in)elastic excitation functions shown in this paper were recorded after instrumental optimization at 13 eV and were uncorrected from the instrument transmission function. For each presented vibrational excitation function (VEF), a background subtraction was performed, although this procedure did not result in significant curve shape changes [14, 23].

The model background contribution was taken as the inelastic excitation function recorded for the energy loss 1000 meV, loss at which no vibrational modes were expected to contribute. The electron-induced damaging of the films during the long accumulation times was regularly checked for.

HREELS energy calibration. When recording a spectrum using the HREEL spectrometer, the "real" or effective impact energy E_{impact} of the incoming electrons onto the sample, referred to sample vacuum energy level E_{vac}, depends on the sample and analyser work functions, respectively Φ_{SAM} and Φ_a, and on the analyser potentials (the potential difference between the sample and the analyser E_i - U_A and the pass energy $E_{pass\ a}$) [24-26].

$$E_{impact} = E_i - U_A + E_{pass\ a} + \Phi_a - \Phi_{SAM} \quad (1)$$

This electron impact energy is determined experimentally from the cut-off peak observed in energy loss spectra recorded at different E_i, at fixed analyser potentials $E_{pass\ a}$ - U_A [27, 28]. Typical values for U_A are $-0.006 \leq U_A \leq 0.03$ V, i.e. negligible with respect to E_i, and $E_{pass\ a} = 1.70$ V. The energy correction is given by $E_{impact} - E_i = 0.71 \pm 0.02$ eV, rounded to 0.7 eV in the following. The work function difference $\Phi_a - \Phi_{SAM}$ is then equal to -0.99 ± 0.02 eV ≈ -1.0 eV. From this value, the work function of the instrument can be estimated at $\Phi_a = 3.3 \pm 0.1$ eV, taking $\Phi_{SAM} = 4.30$ eV for the sample work function [20]. It should be kept in mind that the sample effective work function of a SAM sample is demonstrated to be strongly sensitive to layer defects (variations up to 1 eV were discussed in the case of SAM contamination and thiol molecule orientation defect) [29].

3. Results & discussion

The characteristics of low-energy electron inelastic scattering at substrate surfaces are dictated by a close interplay between: (i) the density-of-states (DOS) of the environment in which the probed species are embedded and (ii) the vibrational excitation mechanisms (dipolar and/or impact scattering including resonant scattering) [30, 31]. The DOS is probed by recording elastic reflectivity curve and is strongly dominated by the molecular layer characteristics as will be discussed in section 3.1. The mechanisms involved in the excitation of representative vibrational modes by electron impact is probed by recording inelastic excitation functions associated to selected energy losses, as presented in section 3.2.

3.1. Elastic reflectivity & DOS above vacuum level

The elastic excitation function, or electron elastic reflectivity, is proportional to the number of quasi-elastically backscattered electrons. As seen in Figure 1 and Figure 2(a) it displays a strong maximum in the range E_i = 6.5 -7.9 eV (E_{impact} = 7.2 - 8.6 eV), followed by a minimum at about 11.5 eV (E_{impact} = 12.2 eV). The electron elastic reflectivity of a substrate probed using HREELS is governed by the probability for electron backscattering from the surface, and thereby relates to the sample DOS above the vacuum level E_{vac} [14, 15]. Local maxima (minima) observed in the electron elastic reflectivity curve can be associated with local minima (maxima) of the sample electronic band structure. When the density of available unoccupied electronic states reaches a minimum, the incoming electrons cannot propagate into the sample, and consequently the elastic scattering probability is strongly enhanced.

The DOS of TPT SAMs above vacuum level is difficult to access either experimentally or theoretically. NEXAFS spectra recorded for TPT SAMs at the Carbon edge between 283 and 310 eV photon energy [16-20] reflect the density of the unoccupied molecular states. All spectra taken at normal incidence agree well with each other. Interestingly, these spectra compare very well with the Carbon K-shell spectrum of gaseous benzene recorded by inner-shell electron energy loss spectroscopy (ISEELS) under electric-dipole conditions (2 keV, small angle) [21]. The precise attributions of the observed features are still under discussion in the literature, and often refer to data available for related molecular systems such as biphenyl SAMs [20], deposited benzenethiol [32], condensed ice layer of deuterated benzene C_6D_6 [33], and gaseous benzene C_6H_6 [21]. The DOS general trends [16-21] between $h\nu \approx 290$ and 302 eV are converted in Figure 1 into intensity of shading. Two DOS maxima are observed centred at $h\nu \approx 293.5$ eV (width 3 eV) and $h\nu \approx 301.5$ eV (very broad), and are separated by a DOS local minimum at $h\nu \approx 296$ eV (width 2 eV).

In order to compare the DOS data obtained by HREELS with the data available from core excitation techniques (NEXAFS and ISEELS), the C(1s) binding energy (BE) reported for TPT SAMs is used as a reference to locate the sample Fermi level [34]. The chosen average value BE = 284.3 eV was estimated from XPS (X-ray Photoelectron Spectroscopy) measurements [16-19]. The vacuum level position E_{vac} could then be obtained by adding the sample work function Φ_{SAM} = 4.30 eV to the Fermi level energy E_F. In practice, the NEXAFS photon energy and the incident electron energy were linked by the following relationship:

$$E - E_{vac} = h\nu - BE - \Phi_{SAM} = h\nu - 288.6 \text{ eV}. \quad (2)$$

The Lowest Unoccupied Molecular Orbital (LUMO) and the Highest Occupied Molecular Orbital (HOMO) calculated for the isolated TPT molecule are respectively located at +2.9 eV

(resp. +2.2 eV) and -1.5 eV (resp. -1.9 eV) with respect to E_F [12] (resp. [35]), both of them are located below the sample vacuum level (Figure 1).

Thanks to the electron incident energy calibration performed (see experimental section), it is possible to plot the HREEL elastic reflectivity curve on the energy scale starting from the vacuum level. As expected, an observed maximum (minimum) in the elastic reflectivity curve can be related to a minimum (maximum) in the NEXAFS and ISEELS curves (Figure 1). The high electron reflectivity region extending from E_{impact} = 7.2 eV up to 8.6 eV, can be related to the DOS local minimum found in NEXAFS at $h\nu \approx 296$ eV. The strong decrease toward lower incident energies is ascribed to the DOS maximum at $h\nu \approx 293.5$ eV. The minimum electron reflectivity located E_{impact} = 12.2 eV corresponds to the DOS local maximum found in NEXAFS at $h\nu \approx 301.5$ eV.

The spectrometer transmission function was optimized at E_i = 13 eV, so that the instrument function would not interfere with the high reflectivity region discussed above. In our previous publication [13], the DOS induced structures were smoothed because the spectrometer optimization procedure was performed at E_i = 3 eV. As a consequence, the reinforced transmission function did compensate for the sample low reflectivity at low energy.

Inelastic scattering for electrons coming in the close vicinity of the substrate suffers substrate reflectivity factors [25, 30]. Therefore, most of the vibrational excitation functions are expected to be significantly modulated. In that respect, the electron high reflectivity window extending from E_i = 6.5 to 7.9 eV is grey shaded in every panel of Figures 2, 3, 4. It is necessary to keep in mind that a relative maximum observed in this region would most probably be related to the local high reflectivity, rather than to an electron attachment resonance.

In conclusion, the specular electron elastic reflectivity measured using HREELS can be directly compared with NEXAFS and ISEEL spectra, which validates the energy calibration performed. The HREEL measurement allows to probe the sample DOS above vacuum level without creating an inner-shell hole, but the reflectivity spectra are obtained over a reduced energy range and do suffer from the influence of the instrument transmission function. The agreement between the DOS structures deduced for TPT SAMs by HREELS and NEXAFS with the ones observed for gaseous benzene using ISEELS is striking. Specular vibrational excitation functions can now be scaled with respect to the SAM vacuum level, and are modulated by DOS related structures and resonant mechanisms.

3.2. Inelastic excitation functions & vibrational excitation mechanisms under electron impact

Extended energy loss spectra were discussed in detail in a previous publication [12]. Based on DFT calculations performed on the isolated molecule, vibrational assignments were proposed. We focus in this paper on the vibrational excitation functions (VEF) recorded for selected energy losses, ascribed to fundamental mode excitations ($\Delta v = 1$, losses at 56, 94, 124, 146, 160, 184, 196, 379 meV), to two-fold successive inelastic scattering events ($2\times\Delta v = 1$, loss at 756 meV), and to overtone excitations ($\Delta v = 2$ and 3, losses at 742 and 1090 meV).

Selected excitation functions of fundamental modes

Electron-induced vibrational excitation of a substrate proceeds through two interaction mechanisms: namely dipolar and impact excitations. Both mechanisms contribute simultaneously, although their relative contributions depend on the scattering conditions, in particular on the incident electron energy and on the considered scattering geometry [30]. Upon dipolar scattering, the excitation of vibrational modes proceeds via the interaction of the incoming electrons with the dynamic dipoles of the substrate. Since the electrons are moving, the sample 'sees' a time-varying field, a mechanism analogue with the vibrational excitation mechanism involved in infrared absorption spectroscopy. The interaction occurs from a relatively large distance (~10-100 Å), and during a rather long time. The probability for vibrational excitation by dipolar scattering continuously decreases with increasing incident electron energy E_i [36]. Upon impact scattering, the vibrational excitation is operative via short-range (~1 Å) interaction mechanisms relying on the direct scattering of the incoming electrons by the substrate atomic potentials. The probability of vibration excitation via impact scattering increases with increasing incident electron energy E_i. A particular case of impact scattering is resonant scattering [36, 37]. It involves the temporary capture of the incident electron into an empty orbital of the sample forming a negative ion resonance. Therefore resonant scattering only takes place in few energy windows, when the incoming electrons have an energy resonant with the energy of the temporarily populated state. Then the vibrational excitation probability is not only enhanced for the fundamental loss, but also for the overtones, corresponding to the excitation of several quanta of vibration through a single inelastic scattering event.

In Figure 2 three VEFs, recorded for three fundamental energy losses, are compared to the elastic reflectivity. Their behaviour as a function of the incident electron energy E_i is strikingly different as will be discussed below. In addition, a large number of vibrational

modes are contributing to the energy loss region 75-200 meV. Most of them are strongly coupled and difficult to describe [12]. In Figure 3 are shown the specular inelastic excitation functions recorded for the losses E_{loss} = 94, 124, 146, 160, 184, and 196 meV. At first glance, they behave globally the same.

The energy loss located at 146 meV is ascribed to mixed in-plane bending δ(CH), stretching ν(CC) and stretching ν(CS) modes. The associated VEF (Figure 2(b)) shows a globally decreasing trend, corresponding to a significant contribution of dipolar excitation mechanism. The superimposed maximum can be directly related to the high reflectivity region (Figure 2(a)). It shows that some electrons have approached close enough the sample to probe its DOS. Thus the impact mechanism is also contributing to the vibrational excitation. The VEF associated to the loss 184 meV (Figure 3(e)) attributed to mixed δ(CH)/ ν(CC) resembles a lot the VEF associated to 146 meV, described just above. These VEFs display a significant dipolar contribution and mimic the electron reflectivity, in accordance with [13].

By contrast, the excitation function recorded for the loss at 56 meV ascribed to out-of-plane modes γ(CH) (Figure 2(c)) shows an increasing general trend, indicating that this mode is dominantly excited by impact scattering. Considering the average orientation of the TPT molecules within the SAM, this mode is mostly associated to dynamic dipoles parallel to the sample surface. Such modes are not efficiently excited by dipolar scattering when the samples are conductive enough. The clear plateau in the excitation function corresponds to the high reflectivity region. A shoulder is seen at about 11.5 eV. The VEF recorded for the loss at 94 meV (Figure 3(a)) and attributed to γ(CH) shows also an increased non-resonant impact mechanism contribution. In the case of the in-plane deformation of the aromatic rings δ_{ph} (E_{loss} = 124 meV, Figure 3(b)), and of δ(CH) (E_{loss} = 160 meV, Figure 3(d)), the high-reflectivity related structure extends and peaks at about ~ 9 eV.

Finally, the VEF recorded at 379 meV for the unresolved modes ν(CH) (Figure 2(d)) again shows a different shape from the other VEFs. A strongly decreasing dependence is observed for increasing incident electron energy, meaning that the dominantly involved excitation mechanism proceeds through dipolar scattering. A superimposed structure peaking around E_i = 6 eV is produced by vibrational excitation through electron attachment, as previously published [13]. In addition to this main resonant process which will be further discussed below, the VEF associated to the stretching modes ν(CC) (E_{loss} = 196 meV, Figure 3(f)) displays a new structure at E_i ~ 10 eV, attributed to an electron attachment resonance. The

involved state(s) could be the analogue(s) of the one(s) predicted between 9 and 11 eV for the gaseous anion $C_6H_6^-$ [38].

Resonant excitation of the unresolved stretching modes ν(CH)

The vibrational excitation of the unresolved stretching modes ν(CH) partly proceeds through electron attachment around 6 eV, and accordingly a series of overtones could be observed at 742 meV and ~1090 meV in the extended energy loss spectra [12]. In Figure 4 are considered the losses 379 meV, 742 meV, 1090 meV and 756 meV, respectively attributed to fundamental excitations $\nu(CH)_{\Delta v = 1}$, first overtone excitations $\nu(CH)_{\Delta v = 2}$, second overtone excitations $\nu(CH)_{\Delta v = 3}$, and two-fold scattering excitations $2 \times \nu(CH)_{\Delta v = 1}$.

The three VEFs recorded at 379, 742, and 1090 meV have the same behavior as a function of the incident electron energy, but with absolute intensities becoming smaller as expected for multiple loss excitation. For the three VEFs, the globally decreasing dependence is attributed to dipolar scattering. The fact that this mechanism is involved in the excitation of overtones can be related to the noticeable anharmonicity of the CH oscillator ($\omega_e = 396.0 \pm 0.6$ meV, $\omega_e x_e = 8.2 \pm 0.3$ meV [12]), softening the $\Delta v = 1$ IR selection rule. The electron attachment resonance contributes to each of these VEFs as a peak around $E_i = 6$ eV.

In the case of the VEF recorded at 756 meV, the dipolar excitation mechanism is almost the only contributing one. No noticeable contribution of impact mechanism is observed, as the resonance has almost vanished. The incoming electrons have to undergo two successive inelastic scattering events (each of them resulting in a loss of about 379 meV) before being detected, which strongly favours the "purely" dipolar scattering events for a detection in the specular direction. This VEF is considered in the following as a model one for dipolar excitation of CH related multiple loss (of the second order).

In an attempt to isolate the electron attachment resonance that is involved, we focussed on the double losses, i.e. the overtone loss at 742 meV, and the multiple loss at 756 meV. The VEF associated to the latter was subtracted from the VEF associated to the former. The resulting curve presented in Figure 4(e) has a clear bell-shape peaking at $E_i = 6.5$ eV, with no background contribution. This procedure was repeated for four different TPT SAMs, and different spectrometer optimizations / recording procedures. The four curves superimpose remarkably well with each other and the average curve is shown in Figure 4(f). After subtraction of the model dipolar vibrational excitation contribution, the purely resonant contribution appears to be centred at $E_i = 6.5$ eV and has a width of 3.4 eV. According to the

energy calibration that was performed, the resonance is located at E_{impact} = 7.2 eV above the sample vacuum level.

The most comprehensive set of data available in the literature deals with benzene in the gas phase. As seen in Figure 1, the resonance is located at the boundary of the high reflectivity / low DOS region of the SAM sample. In this region, for the benzene molecule, a faint structure (labelled G) was seen in the ISEEL spectrum and molecular excited states were theoretically predicted [21]. The latter were doubly excited states involving molecular orbitals having π^* and CH antibonding characters. In addition, an electron attachment resonance was observed at ~8.0 eV through the two competitive decay channels [39]: (i) electron autodetachment leaving the system in a vibrational excited state, and (ii) dissociative electron attachment leading to the formation of anionic and neutral fragments. A very broad $\sigma^*_{C\text{-}H}$ shape resonance, probably formed by one or more resonance states was observed between 4 and 10 eV in vibrational excitation of the electronic ground state of C_6H_6. It led to a broad structure centred around 8.0 eV (width of ~3 eV) in the excitation function of the modes ν(CH) (E_{loss} = 380 meV) [38], and around ~8.5 eV in the VEFs attributed to $\nu(CH)_{\Delta v = 2}$ (E_{loss} = 0.75 eV) and $\nu(CH)_{\Delta v = 3}$ (E_{loss} = 1.10 eV) [40, 41]. This resonance was also noticed in the total negative ion cross section (width 2.2 eV) [38]. It was observed at about 8 eV and 9 eV in the ion yield curves of the fragment ions $C_6H_5^-$ (width ≤ 0.5 eV) and $C_2H_2^-$ (width ~2 eV), respectively [42]. It would be interesting to perform Electron Stimulated Desorption measurements on the TPT SAMs to probe for possible dissociative relaxation pathways of the identified resonance. Taking into account the energy shift of ~ -1 eV induced by condensed phase effects [9, 11, 25, 43], the TPT SAM resonance energy matches remarkably well with the resonance observed for gaseous benzene. The width evaluated to 3.4 eV is in a good agreement with the width measured in the gas phase for vibrational excitation. Therefore, the TPT SAM behaviour can be assimilated to what would be observed for a model three layer film of benzene molecules condensed at low temperature. There, the phenyl rings would be all up-right oriented on average, as expected from the carbon skeleton of the TPT molecule. Such an organized phase of edge-on adsorbed benzene molecules was studied by Günster et al. upon adsorption on Mo(100) at 100 K [43]. The idea that the TPT SAMs are behaving quite like an assembly of independent (isolated) benzene molecules is in accordance with the calculations performed on the isolated TPT molecule where non-planar equilibrium geometries were predicted, which corresponds to a certain decoupling of the phenyl rings of the chain [12]. Furthermore, a remarkably good agreement was obtained between the IR spectrum simulated for an isolated

TPT molecule and the experimental vibrational spectrum recorded for a TPT SAM [12]. This demonstrated in particular that the intermolecular forces acting within the SAM and the TPT molecule-substrate interaction are not strong enough to perturb significantly the observed HREEL signatures.

4. Conclusion

Low energy electron scattering on TPT SAMs was investigated using HREELS by recording elastic and inelastic excitation functions. Thanks to the energy calibration that was performed, the electron energy could be referred to the SAM vacuum level. A high elastic reflectivity region was observed between E_{impact} = 7.2-8.6 eV, attributed to a minimum DOS observed by NEXAFS. Inelastic vibrational excitation functions were recorded for a selection of vibrational modes, in order to get insights about the vibrational excitation mechanisms induced by electrons (dipolar and impact scattering). In particular, the excitation of the modes ν(CC) (196 meV) and ν(CH) (379 meV) involved electron attachment resonances. For the stretching modes ν(CH), the resonant contribution could be extracted from the overtone excitation. The resonance is located at E_{impact} = 7.2 eV above the vacuum level (FWHM = 3.4 eV), and its nature was discussed considering the comprehensive set of data available in the literature for gaseous benzene.

Acknowledgments

We thank Dr. Christophe Poulard for his help for the UV-Ozone treatment. We acknowledge the financial support by C'Nano, Ile-de-France, Programme Francilien de Recherche en Nanosciences, through the 2009 SAMTOX-NC granted project. This work was conducted within the framework of the COST action CM1301 (CELINA for 'Chemistry for ELectron-Induced Nanofabrication') and the ANR-DFG 2014 HREELM project. The acquisition of the HREELS equipment at the LCAM-ISMO was financially supported by Conseil Général de l'Essonne and by the LabEx PALM "ProDaC" project.

Figure 1

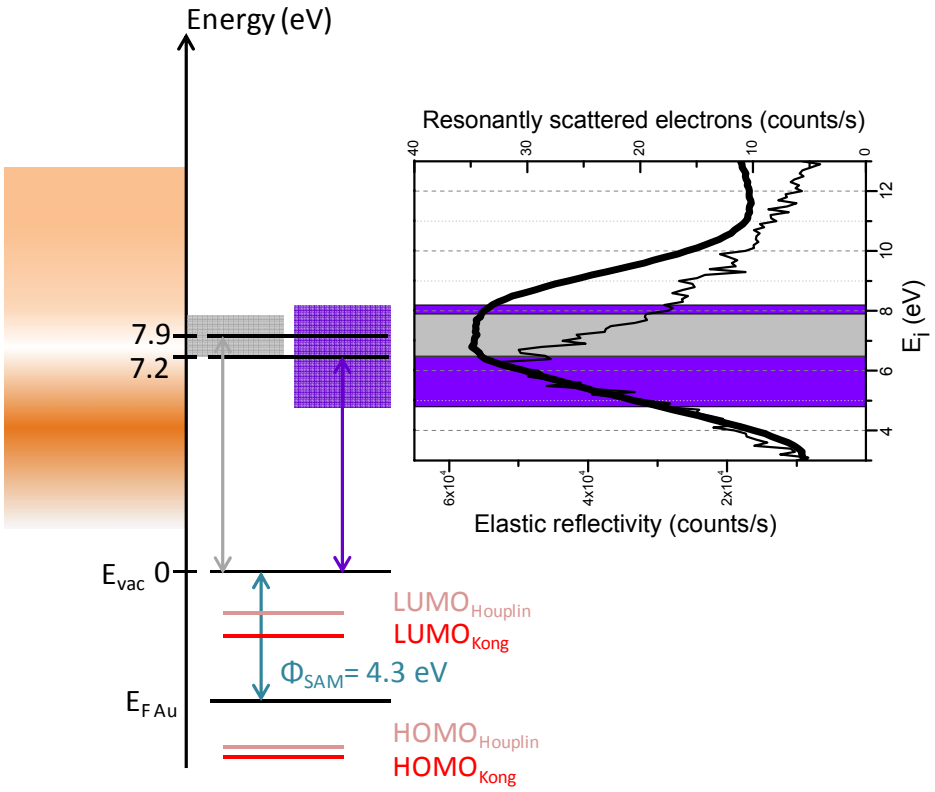

Figure 1:

TPT SAM electron elastic reflectivity compared to DOS qualitative representations. The energy reference is the sample vacuum level E_{vac} = 0 eV, located 4.3 eV above the Fermi level E_F [20]. The incident electron energy E_i was converted into an effective impact energy E_{impact} to position the measured elastic reflectivity curve (thick black curve on the right hand side, lower axis, width represented in grey) with respect to E_{vac}. This curve is also shown in Figure 2 (a). LUMO and HOMO calculated for the isolated TPT molecule [12, 35] are positioned with respect to the Fermi Level. The general trend found for DOS, as deduced from compared NEXAFS [16-20] and ISEELS [21] measurements, was converted into intensity of the shading, the latter being directly related to the observed DOS (on the left hand side). Also represented an estimate of the resonant contribution to vibrational excitation of the modes ν(CH) (thin black curve on the right hand side, upper axis, width represented in purple), curve also shown in Figure 4 (f).

Figure 2

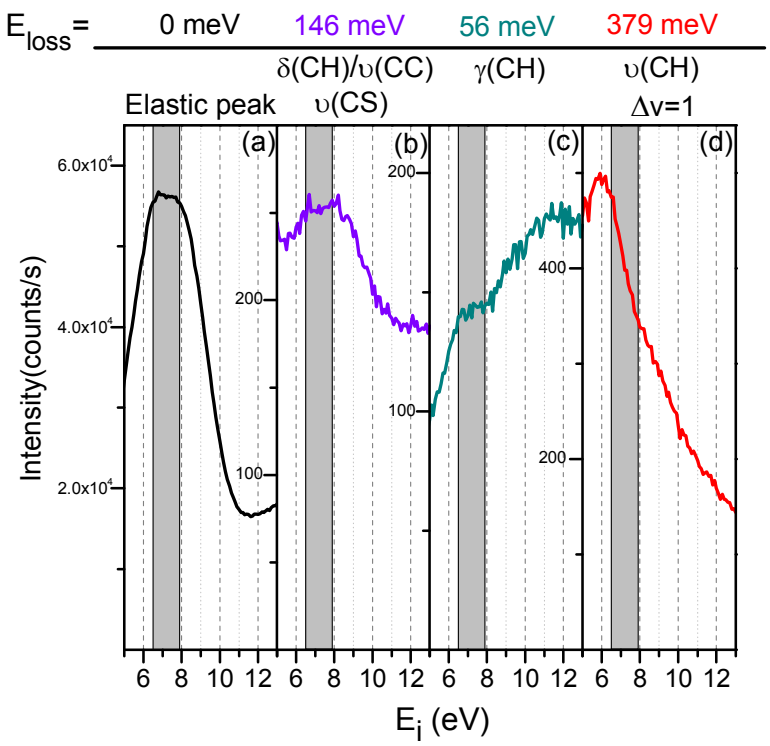

Figure 2: Specular electron elastic reflectivity recorded over the range 5-13 eV for incident electron energy E_i (a) (already shown in Figure 1). Specular inelastic excitation functions recorded for selected losses: E_{loss} = 146 (b), 56 (c), and 379 meV (d). The shaded energy windows correspond to the electron reflectivity maximum.

Figure 3

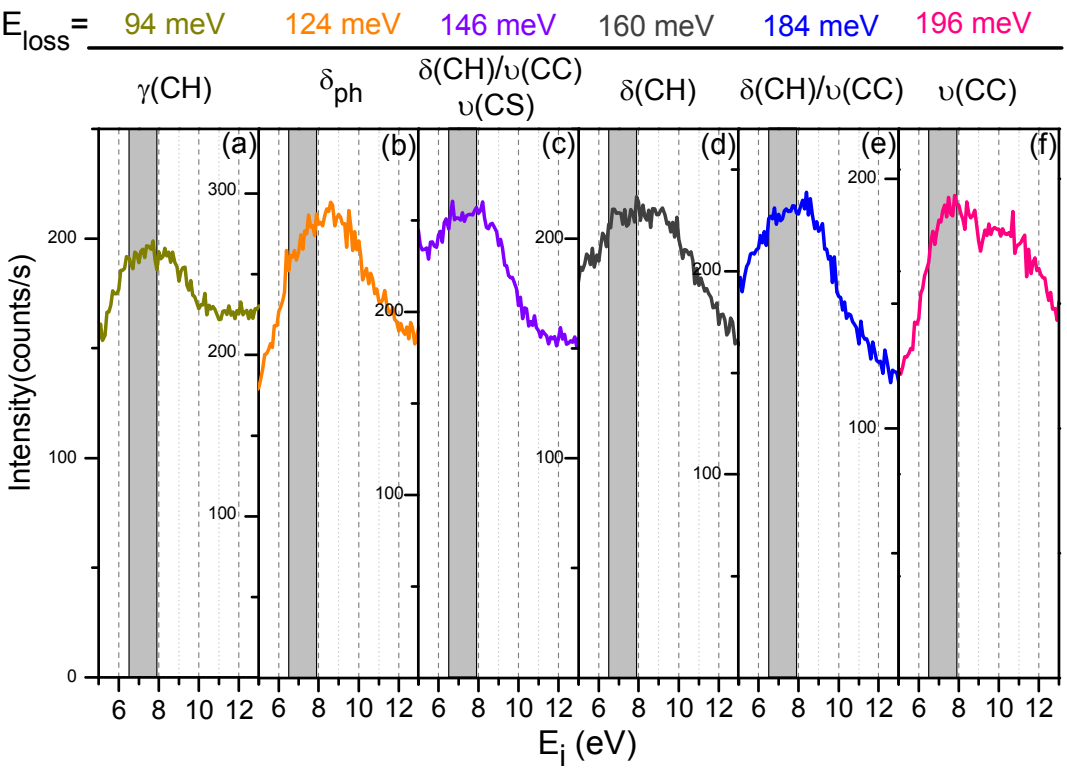

Figure 3: Specular inelastic excitation functions recorded for selected losses: E_{loss} = 94 (a), 124 (b), 146 (c) (already shown in Figure 2(b)), 160 (d), 184 (e), and 196 meV (f). The shaded energy windows correspond to the electron reflectivity maximum.

Figure 4

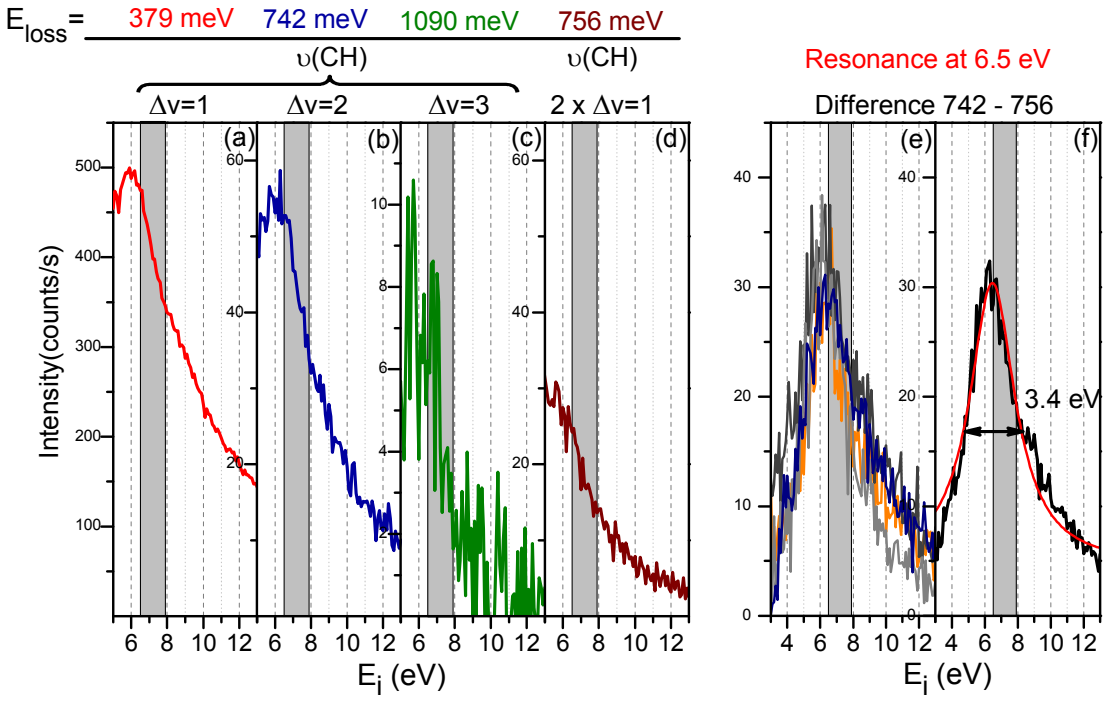

Figure 4: Excitation functions recorded for the losses 379 meV (a), 742 meV (b), 1090 meV (c) and 756 meV (d), respectively attributed to fundamental excitations $\nu(CH)_{\Delta v=1}$, first overtone excitations $\nu(CH)_{\Delta v=2}$, second overtone excitations $\nu(CH)_{\Delta v=3}$, and two-fold scattering excitations $2 \times \nu(CH)_{\Delta v=1}$. In an attempt to isolate the electron attachment resonance that is involved, the VEF associated to the multiple loss at 756 meV was subtracted from the VEF associated to the overtone loss at 742 meV. This procedure was repeated for four different TPT SAMs, and different spectrometer optimizations / recording procedures. The four curves (panel e) superimpose remarkably well with each other and the average curve is shown in panel (f), compared to the DOS in Figure 1. It was fitted using a bell-shape curve centred at 6.5 eV and having a FWHM = 3.4 eV (Lorentzian) to guide the eye.

References

[1] J.C. Love, L.A. Estroff, J.K. Kriebel, R.G. Nuzzo, G.M. Whitesides, *Chem. Rev.* 2005, **105,** 1103-1169. Self-Assembled Monolayers of Thiolates on Metals as a Form of Nanotechnology.

[2] F. Schreiber, *J. Phys.: Condens. Matter* 2004, **16,** R881-R900. Self-assembled monolayers: from 'simple' model systems to biofunctionalized interfaces.

[3] P. Angelova, H. Vieker, N.-E. Weber, D. Matei, O. Reimer, I. Meier, S. Kurasch, J. Biskupek, D. Lorbach, K. Wunderlich, L. Chen, A. Terfort, M. Klapper, K. Müllen, U. Kaiser, A. Gölzhäuser, A. Turchanin, *ACS Nano* 2013, **7**, 6489-6497. A universal scheme to convert aromatic molecular monolayers into functional carbon nanomembranes.

[4] N. Meyerbroeker, P. Waske, M. Zharnikov, *J. Chem. Phys.* 2015, **142,** 101919. Amino-terminated biphenylthiol self-assembled monolayers as highly reactive molecular template.

[5] A. Turchanin, A. Gölzhäuser, *Prog. Surf. Sci.,* 2012, **87**, 108-162. Carbon nanomembranes from self-assembled monolayers: Functional surfaces without bulk.

[6] Z. She, A. DiFalco, G. Hähner, M. Buck, *Beilstein J. Nanotechnol.*, 2012, **3**, 101–113. Electron-beam patterned self-assembled monolayers as templates for Cu electrodeposition and lift-off.

[7] A. Turchanin, D. Käfer, M. El-Desawy, C. Wöll, G. Witte, A. Gölzhäuser, *Langmuir,* 2009, **25**, 7342–7352. Molecular mechanisms of electron-induced cross-linking in aromatic SAMs.

[8] B. Völkel, A. Gölzhäuser, H.U. Müller, C. David, M. Grunze, *J. Vac. Science & Technol. B*, 1997, **15**, 2877-2881. Influence of secondary electrons in proximal probe lithography.

[9] C.R. Arumainayagam, H.-L. Lee, R.B. Nelson, D.R. Haines, R.P. Gunawardane, *Surf. Sci. Reports*, 2010, **65**, 1-44. Low-energy electron-induced reactions in condensed matter.

[10] E. Böhler, J. Warneke, P. Swiderek, *Chem. Soc. Rev.*, 2013, **42**, 9219-9231. Control of chemical reactions and synthesis by low-energy electrons.

[11] I. Bald, J. Langer, P. Tegeder, O. Ingolfsson, *Int. J. Mass Spectrom.*, 2008, **277**, 4-25. From isolated molecules through clusters and condensates to the building blocks of life, A short tribute to Prof. Eugen Illenberger's work in the field of negative ion chemistry.

[12] J. Houplin, L. Amiaud, T. Sedzik, C. Dablemont, D. Teillet-Billy, N. Rougeau, A. Lafosse, *Eur. Phys. J. D.*, 2015, DOI: 10.1140/epjd/e2015-60240-3. A combined DFT / HREELS study of the vibrational modes of terphenylthiol SAMs.

[13] L. Amiaud, J. Houplin, M. Bourdier, V. Humblot, R. Azria, C.-M. Pradier, A. Lafosse, *Phys. Chem. Chem. Phys.*, 2014, **16**, 1050-1059. Low-energy electron induced resonant loss of aromaticity: consequences on cross-linking in terphenylthiol SAMs.

[14] A. Lafosse, D. Cáceres, M. Bertin, A. Hoffman, R. Azria, *Surf. Sci.*, 2005, **587**, 134–141. Role of electronic band structure and resonances on electron-scattering. The case of the hydrogenated polycrystalline diamond.

[15] A. Lafosse, A. Hoffman, M. Bertin, D. Teillet-Billy, R. Azria, *Phys. Rev. B*, 2006, **73**, 195308. Density-of-states effect on surface and lattice vibrational modes in hydrogenated polycrystalline diamond.

[16] S. Frey, V. Stadler, K. Heister, W. Eck, M. Zharnikov, M. Grunze, *Langmuir*, 2001, **17**, 2408-2415. Structure of Thioaromatic Self-Assembled Monolayers on Gold and Silver.

[17] C. Fuxen, W. Azzam, R. Arnold, G. Witte, A. Terfort, C. Wöll, *Langmuir*, 2001, **17**, 3689-3695. Structural characterization of organothiolate adlayers on gold: the case of rigid aromatic backbones.

[18] H.-J. Himmel, A. Terfort, C. Wöll, *J. Am. Chem. Soc.*, 1998, **120**, 12069-12074. Fabrication of carboxyl-terminated organic surface with self-assembly of functionalized terphenylthiols: the importance of hydrogen bond formation.

[19] M. Zharnikov, M. Grunze, *J. Phys.: Condens. Matter*, 2001, **13**, 11333-11365. Spectroscopic characterization of thiol-derived self-assembling monolayers.

[20] D. Käfer – PhD dissertation, Department of Physical Chemistry I, Ruhr-University Bochum, 2008, Characterization and optimization of growth and electronic structure of organic thin films for applications in organic electronics.

[21] D. Duflot, J.-P. Flament, J. Heinesch, M.-J. Hublin-Franskin, *J. Electron Spectrosc. Relat. Phenom.*, 2000, **113**, 79-90. Re-analysis of the K-shell spectrum of benzene.

[22] http://arrandee.com/usage.html

[23] A.T. Wen, M. Michaud, L. Sanche, *Phys. Rev. A*, 1996, **54**, 4162-4170. Observation of temporary-negative-ion states in condensed methanol via vibrational excitation induced by slow electron scattering.

[24] IB 500 User's Guide, version 1.0, Omicron, June 2000, p20.

[25] G.D. Waddill, L.L. Kesmodel, *Phys. Rev. B*, 1985, **32**, 2107. Benzene chemisorption on palladium surfaces. II. Resonance electron scattering and overtone vibrations.

[26] M. Rocca, F. Moresco, *Phys. Rev. B*, 1994, **50**, 18621. LEED fine structures and trapping phenomena in inelastic scattering of electrons off Ag(001) and Ag(110).

[27] M. Rei Vilar, G. Horowitz, P. Lang, O. Pellegrino, A. M. Botelho do Rego, *Adv. Mater. Opt. Electron.*, 1999, **9**, 211-218. Surface analysis of Oligothiophene films using HREELS: molecular orientation effects.

[28] J. Houplin – PhD dissertation, Ecole doctorale de Chimie de Paris Sud ED470, Université Paris Sud, 2015, Structuration chimique induite et contrôlée par impact d'électrons lents sur films moléculaires supportés.

[29] D. Fragouli, T.N. Kitsopoulos, L. Chiodo, F. Della Sala, R. Cingolani, S.G. Ray, R. Naaman, *Langmuir* , 2007, **23**, 6156-6162. Imaging Photoelectron Transmission through Self-Assembled Monolayers: The Work-Function of Alkanethiols Coated Gold.

[30] A. Lafosse, R. Azria, Chap. 7 in "Low-Energy Electron Scattering from Molecules, Biomolecules and Surfaces", CRC Press Taylor & Francis Group, Editors P. Čársky & R. Čurík (2012). "Low-energy electron scattering at surfaces."

[31] R. Azria, A. Lafosse, L. Amiaud, Sh. Michaelson, A. Hoffman, *Progress in Surf. Sci.*, 2011, **86**, 94–114. Hydrogenated polycrystalline diamond films: Elastic and inelastic electron reflectivity.

[32] J. Stohr, D.A. Outka, *Phys. Rev. B*, 1987, **36**, 7891-7905. Determination of molecular orientations on surfaces from the angular dependence of near-edge x-ray-absorption fine-structure spectra.

[33] D. Menzel, G. Rocker, H.-P. Steinrück, D. Coulman, P.A. Heimann, W. Huber, P. Zebisch, D.R. Lloyd, *J. Chem. Phys.*, 1992, **96**, 1724-1734. Core excitation, decay, and fragmentation in solid benzene as studied by x-ray absorption, resonant Auger, and photon stimulated desorption.

[34] H. Okuyama, H. Kato, M. Kawai, J. Yoshinobu, *J. Chem. Phys.*, 2000, **113**, 2866-2872. An electron energy loss spectroscopy study of resonance population in ethylene chemisorbed on Pd(110).

[35] L. Kong, F. Chesneau, Z. Zhang, F. Staier, A. Terfort, P.A. Dowben, M. Zharnikov, *J. Phys. Chem. C*, 2011, **115**, 22422-22428. Electronic structure of aromatic monomolecular films: The effect of molecular spacers and interfacial dipoles.

[36] P.A. Thiry, M. Liehr, J.J. Pireaux, R. Caudano, *Phys. Scr.*, 1987, **35**, 368-379. Electron interaction mechanisms in High Resolution Electron Energy Loss Spectroscopy.

[37] R.E. Palmer, P.J. Rous, *Rev. Mod. Phys.*, 1992, **64**, 383-440. Resonances in electron scattering by molecules on surfaces.

[38] R. Azria, G.J. Schulz, *J. Chem. Phys.*, 1975, **62**, 573-575. Vibrational and triplet excitation by electron impact in benzene.

[39] M. Allan, *J. Physics: Conf. Series*, 2012, **388**, 012001. Measuring and modeling absolute data for electron-induced processes.

[40] M. Allan, *J. Electron Spectrosc. Rel. Phenom*., 1989, **48**, 219-351. Study of triplet states and short-lived negative ions by means of electron impact spectroscopy.

[41] M. Ben Arfa, M. Tronc, *J. Electron Spectrosc. Rel. Phenom.*, 1990, **50**, 117-128. Symmetry selection rules versus vibronic coupling in resonant selective vibrational excitation of polyatomic molecules by electron impact.

[42] H.-P. Fenzlaff, E. Illenberger, *Int. J. Mass Spectrom. & Ion Process.*, 1984, **59**, 185-202. Low energy electron impact on benzene and the fluorobenzenes. Formation and dissociation of negative ions.

[43] J. Günster, J. Stultz, S. Krischok, D.W. Goodman, *Chem. Phys. Lett.*, 1999, **306,** 335–340. Two- to three-dimensional transition intermediate: growth of benzene on Ru(001) and Mo(100).